

Application of X-ray Photoelectron Spectroscopy (XPS) for the Surface Characterization of Gunshot Residue (GSR)

A. J. “Skip” Schwoeble, Brian R. Strohmeier,* Kristin L. Bunker, Darlene R. McAllister, James P. Marquis, Jr., John D. Piasecki, and Nikki M. McAllister

RJ Lee Group, Inc., 350 Hochberg Road, Monroeville, PA 15146

* brian.strohmeier@thermofisher.com

Introduction

Gunshot residue (GSR) is typically found on the hands or clothing of persons who have been in the environment of a discharging firearm, but it may also be found on objects in the vicinity of the discharge. Computer-controlled scanning electron microscopy (CCSEM) is the method preferred by the forensic community for the automated analysis of GSR [1–5]. GSR samples are therefore typically collected from a crime suspect’s hands and/or clothing using SEM sample stubs coated with a conductive adhesive. The three major components in modern firearm cartridge primers are lead styphanate (initiator), antimony sulfide (fuel), and barium nitrate (oxidizer) [6]. GSR consists of the products of combustion of these primer materials. Large populations of particles in the size range of ~1–10 μm are rapidly screened by energy-dispersive X-ray spectroscopy (EDS) for the presence of combinations of Pb, Sb, and Ba. When combinations of these three elements are detected, the particles are flagged as potential GSR particulate. Flagged particles with significant Pb/Sb/Ba compositions are subsequently relocated for a live identification and a positive confirmation of GSR. Positive particles are classified as being either “characteristic of GSR” (that is, all three key elements are present) or “consistent with GSR” (that is, any two of the key elements are present) based on the particle composition and morphology. Classification is based on the presence of the constituent elements and is not dependant on the element amounts. If a particle does not meet the proper compositional or morphological criteria, it is rejected as GSR. However, CCSEM generally does not provide information regarding the population of particles much less than 1 μm or the surface chemistry of the GSR particles. This article examines the fine fraction of GSR particles with high-resolution electron microscopy and complements the microscopy data with surface chemistry information from X-ray photoelectron spectroscopy (XPS).

XPS is an ideal analytical technique for investigating the surface chemistry of GSR particles to provide valuable complementary information to SEM/EDS studies. XPS is a qualitative and quantitative surface analysis technique with a sampling depth of \leq ~10 nm [7]. XPS can detect all elements, except for hydrogen and helium, and has a detection limit of ~0.05–0.1 atomic percent for most elements. In addition to elemental surface composition, XPS can reveal unique information about oxidation state and chemical bonding that is unavailable from other techniques [7]. Lastly, XPS can be combined with ion beam sputtering to produce in-depth compositional profiles and chemical state information. Because of its limited spatial resolution compared to electron microscopy techniques, XPS

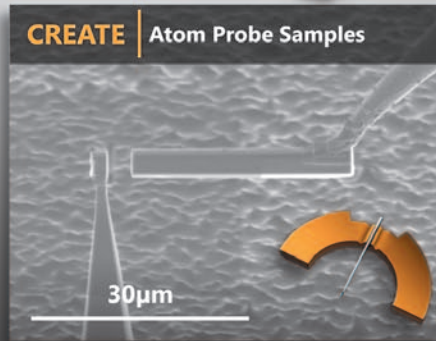
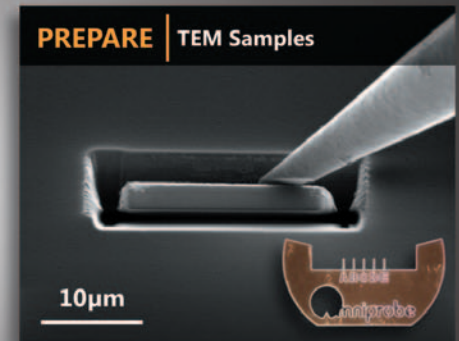
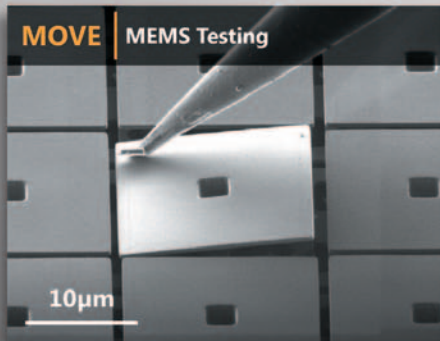
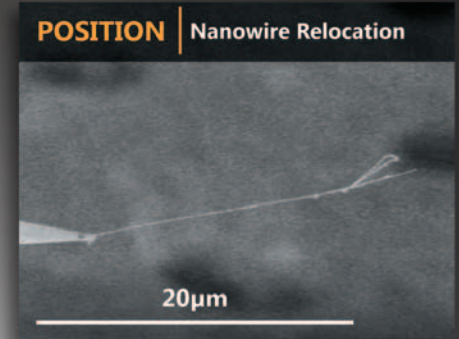
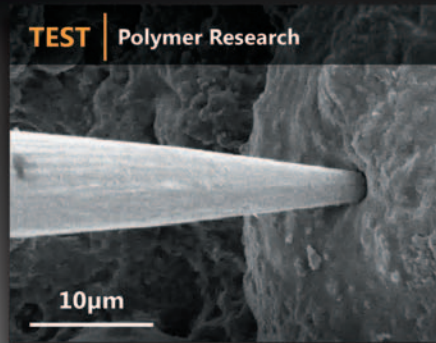
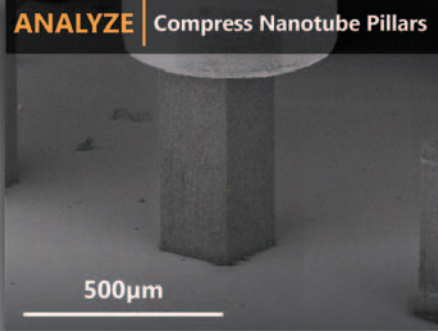
is sometimes not considered a “nanoscale analysis method.” XPS can, however, provide a great deal of information on nanoparticle powders regarding elemental distributions, layer or coating structure and thickness, surface functionality, oxidation state, and chemical bonding that may not be readily available from other methods [8, 9]. One limitation of using XPS to analyze GSR particles is the typical spatial resolution of the technique (for example, > 10 μm). Therefore, XPS cannot be used to obtain surface chemistry from small single particles, but it can be used to determine the surface chemistry of aggregates of small particles or the larger individual particles that are often found in GSR [10].

Despite its many advantages and unique capabilities as a surface analytical technique, XPS has not been widely used in forensic science [11]. A review of the literature found only one published article on the use of XPS for the characterization of GSR in combination with SEM/EDS and atomic force microscopy (AFM) [12]. Our laboratory recently investigated the use of XPS in conjunction with SEM/EDS for characterizing GSR [10]. Time-of-flight secondary ion mass spectrometry (ToF-SIMS) has also been used to investigate the elemental and molecular ion surface composition of GSR in combination with SEM/EDS [13, 14]. XPS, however, potentially offers more information concerning Pb/Sb/Ba surface chemistry of GSR compared to ToF-SIMS because the data obtained on GSR by ToF-SIMS contains mostly elemental information [13, 14].

Materials and Methods

The projectile and gunpowder were removed from a Federal brand 9-mm cartridge so that “primer-only” GSR would be produced when the cartridge was discharged. The primer-only test, although lacking the exposure to high pressure found in a weapon, allows examination of a known primer and only that primer’s spent components. The cartridge was discharged through a 76-mm stainless steel tube placed directly over an alumina ceramic substrate (2 cm dia.). This “direct-deposit” discharge produced a relatively dense layer of GSR particulate of various sizes and shapes on the ceramic substrate surface as shown in Figure 1. The backscattered electron (BSE) image in Figure 1 was obtained with an RJ Lee Instruments SEM.

The GSR deposit was prepared for electron microscopy analysis by first dispersing a portion of the material from the ceramic substrate in filtered isopropanol using ultrasonic agitation. A lacey Formvar/carbon substrate supported by a TEM grid was then dipped in the solution, and the sample was air-dried and further dried on a hot plate at 70°C for 20 minutes. The GSR sample was characterized using a Hitachi



Benefits Include: Port-Mounted, Frees Stage & Chamber Space |
Move Linearly in ANY Direction with Nanometer Precision | Change Tips without Venting |
Quickly Reorient Samples In Situ | Perform Electrical & Nanomechanical Testing
| Easily Perform Nanomanipulation Tasks

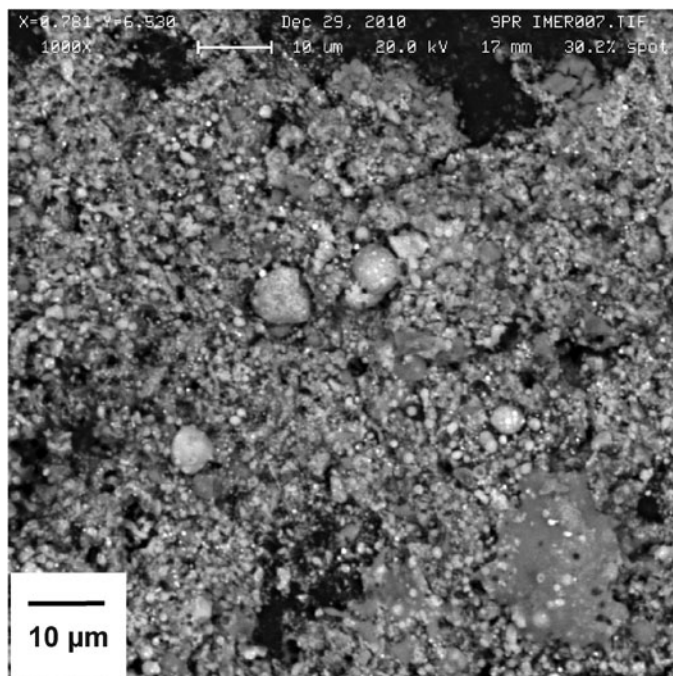


Figure 1: BSE image of the direct-deposit GSR layer on a ceramic substrate.

S-5500 high-resolution field emission SEM with scanning transmission electron microscopy (STEM) capabilities. The analysis was performed at 2 kV to obtain surface morphology information and at 10 kV to obtain elemental maps. The Hitachi S-5500 was equipped with a Bruker EDS system, incorporating a 30 mm² silicon drift detector (SDD). The GSR powder was also analyzed in a Hitachi HD-2300-dedicated 200-kV STEM. The Hitachi HD-2300 was equipped with a lithium-drifted silicon Thermo Scientific EDS system.

XPS analyses were performed with a Thermo Scientific Model K-Alpha XPS instrument. The typical base pressure of the XPS instrument was 2×10^{-9} mbar in the analysis chamber. The XPS instrument utilizes a monochromatic Al K α X-ray source and a low-energy electron/argon ion flood gun for sample charge compensation. The X-ray spot size on the K-Alpha instrument can be varied as necessary from 30–400 μm . The entire ceramic substrate was inserted into the K-Alpha instrument, and XPS analyses were performed directly on one of the heavy GSR deposit areas shown in Figure 1 using a 200- μm X-ray spot size. XPS survey spectra (0–1350 eV binding energy) were obtained to provide qualitative and quantitative elemental surface information. High-resolution XPS spectra were obtained for the major photoelectron peaks of all elements detected in the survey spectra to provide chemical state information. All binding energies were referenced to the main hydrocarbon C 1s peak = 285.0 eV. Surface composition results were calculated from the appropriate peak areas and relative elemental sensitivity factors supplied by the instrument manufacturer. In-depth elemental profile analyses were performed by sputtering with a 1-kV argon ion beam that was rastered over a 2 mm \times 4 mm area. The reported sputtered depths were calibrated using a 100-nm SiO₂ on Si wafer standard reference material.

Results and Discussion

The elemental composition of GSR particles may vary depending on the ammunition used, but the mechanism of particle formation is generally accepted in the forensic science community [5]. GSR particles are formed by the rapid cooling of vaporized Pb, Sb, and Ba following the high-temperature combustion of the primer components. Hence, GSR particles take on characteristic morphologies [5]. For example, GSR particles are generally spherical in shape; however, irregularly shaped particles are often found as well. Particle sizes generally range in size from 1 to 10 μm , although larger and smaller particles are also formed. GSR particles usually have an outer layer of Pb surrounding an inner core of Sb and Ba [5].

A secondary electron image (Hitachi S-5500) of a typical GSR particle acquired at 2 kV is shown in Figure 2. The ~900-nm primary particle shown in Figure 2 was confirmed as GSR following EDS analysis. Other primary particles examined in this study that were confirmed as GSR by EDS ranged in size from ~400 nm to 1 μm . Numerous smaller particles (≤ 50 nm) were typically associated with the larger primary particles as shown in Figure 2. Bright-field STEM (BF-STEM) images (Hitachi HD-2300) of GSR particles and the associated smaller particles were also collected at 200 kV as shown in Figure 3. The thickness of the larger particles was such that no internal structure was visible in the STEM images. There was also little internal structure observed in the bright-field STEM images of the smaller particles. Figure 4 shows a BF-STEM image of a 200-nm GSR particle with smaller particles on the order of 50 nm dispersed around it. The 200-nm particle was identified as characteristic of GSR, whereas the smaller particles were only Pb-rich. Therefore, the smaller particles would not be considered GSR. Similar results were obtained for other particle aggregates with the larger particles (≥ 200 nm) usually being characteristic of GSR and the smaller particles being composed of Pb without Sb or Ba.

Figure 5 shows an XPS survey spectrum, obtained for a 200- μm area on the GSR layer that was deposited on the ceramic substrate for the as-received sample, and a survey



Figure 2: Secondary electron image of a typical GSR particle showing associated smaller particles.

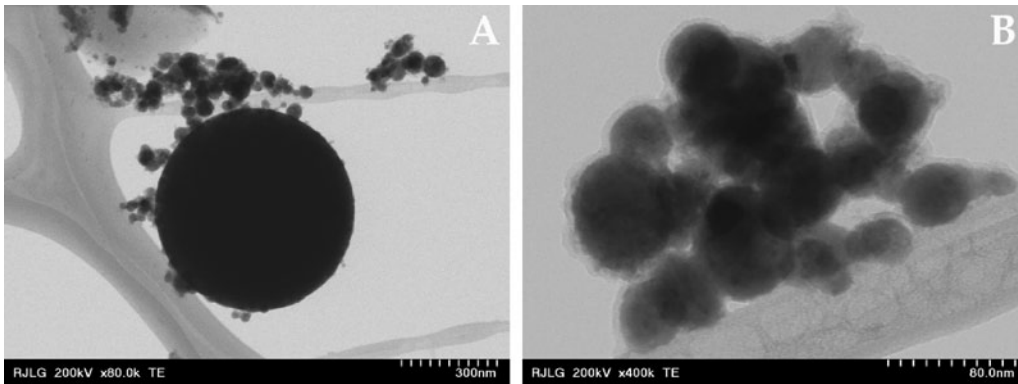


Figure 3: Bright-field STEM (BF-STEM) images of a GSR particle and associated smaller particles dispersed on a lacey carbon grid.

spectrum following argon ion etching 10 nm into the surface. The XPS analysis represents an average surface composition over multiple GSR and associated particles of various sizes contained in the area under the irradiating X-ray spot. The qualitative and quantitative surface composition results are summarized in Table 1 for these two survey spectra as well as for the same area after argon ion sputtering 20 nm in-depth. The survey spectra indicated that the major elemental

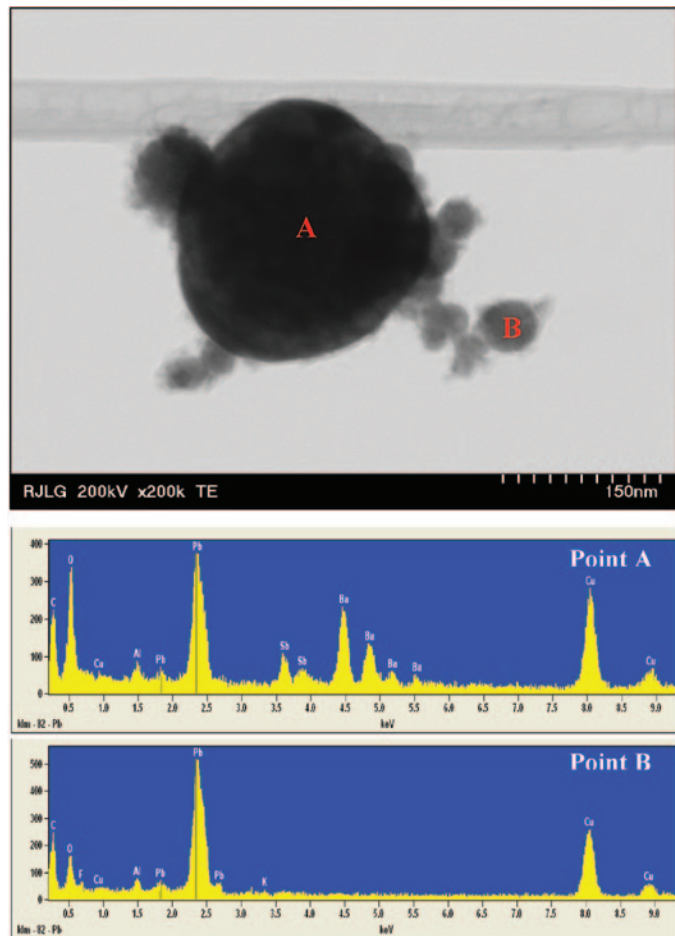


Figure 4: Bright-field STEM (BF-STEM) image and corresponding EDS spectra for a GSR particle and an associated smaller Pb-rich particle dispersed on a carbon lacey grid.

components detected by XPS in the GSR layer were C and O, plus small amounts of Pb, Sb, Ba, and S. No Al from the alumina substrate was detectable, which indicates that the chosen analysis area was completely covered by GSR and that the thickness of the GSR layer was greater than the sampling depth of XPS. Sulfur is a common component in GSR because the fuel used in ammunition primer is antimony sulfide (Sb_2S_3). The amounts of sulfur detected

in the GSR sample in this study were too low to allow an accurate chemical state assignment; however, a previous study indicated that sulfur can be present in GSR as sulfate and sulfide species [10]. The surface concentrations of Sb and Ba increased relative to Pb with the sputtered depth (see Table 1). This finding is consistent with previous XPS results [10] and indicates that, on average, GSR consists of particles with a Pb-rich surface layer and a Sb/Ba-rich core.

In addition to the surface analysis and in-depth elemental profile information discussed above, XPS can also provide

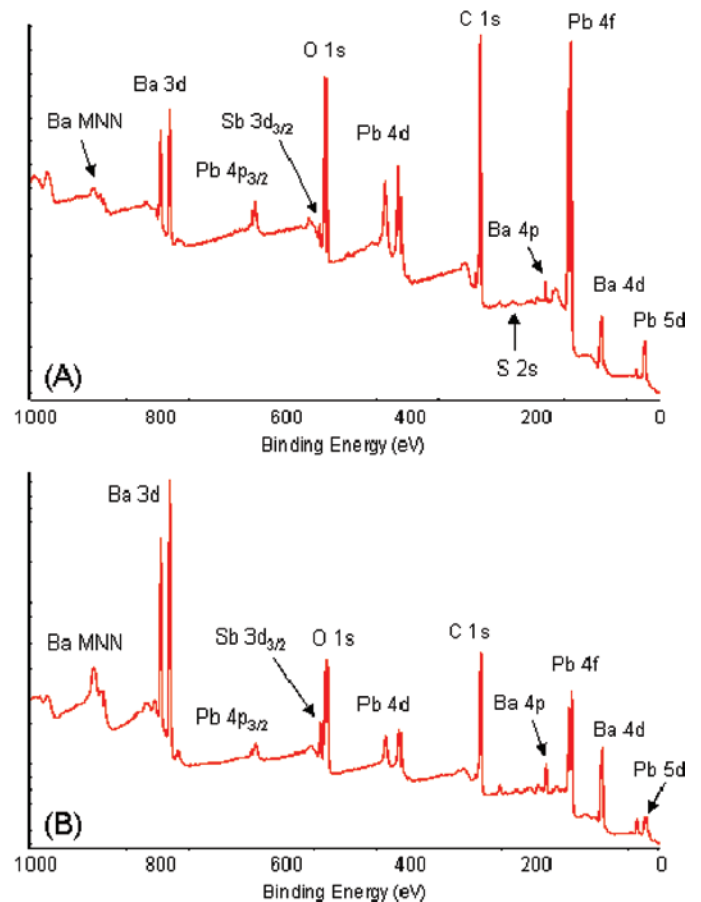


Figure 5: XPS survey spectra for a direct-deposit GSR layer on a ceramic substrate: (A) as-received and (B) after argon ion sputtering 10 nm in-depth.

Table 1: Surface compositions (atomic %) of a direct-deposit GSR sample on a ceramic substrate as determined by XPS before and after argon ion sputtering.

Sample	C	O	S	Sb	Ba	Pb
As-received	69.0	23.2	1.2	0.2	1.6	4.8
Argon ion sputtered 10 nm in-depth	63.2	26.2	0.5	0.6	5.8	3.7
Argon ion sputtered 20 nm in-depth	57.8	30.3	0.3	0.7	7.5	3.4

unique chemical state information for many types of materials, including GSR. Binding-energy information for the main XPS peaks for Pb, Sb, and Ba, and the corresponding chemical state assignments for these elements are summarized in Table 2. Figure 6 shows high-resolution Pb 4f spectra obtained from GSR on a ceramic substrate sample as-received and after argon ion sputtering to depths of 10 nm and 20 nm. The Pb 4f XPS peak appears as a doublet (corresponding to the Pb 4f_{7/2} and Pb 4f_{5/2} electron energy levels) because of spin-orbit splitting for each chemical species present [7, 15]. The Pb 4f spectrum obtained for the as-received sample showed two main peaks (that is, Pb 4f_{7/2} and Pb 4f_{5/2}). Three types of lead oxide are known to exist: PbO (Pb²⁺), Pb₂O₃ (Pb³⁺), and PbO₂ (Pb⁴⁺). XPS can distinguish between these three possibilities because of “chemical shifts” in the Pb 4f binding energies for these different Pb oxidation states [15, 16]. The Pb 4f binding energies observed for the as-received GSR sample were characteristic of PbO [15, 16]. Weak shoulders at binding energies corresponding to Pb metal [15, 16] were observed on the low-binding-energy side of the main Pb 4f peaks for PbO after ion beam sputtering of the sample. The relative amount of Pb metal versus PbO increased slightly with the sputtered depth.

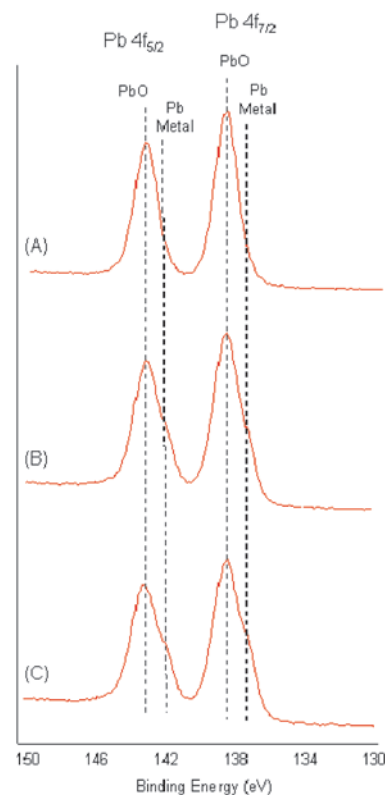
Figure 7 shows representative high-resolution Sb 3d, O 1s, Ba 3d, and X-ray induced Ba MNN Auger spectra obtained for the GSR on a ceramic substrate sample after argon ion sputtering to a depth of 20 nm. No significant differences were observed between these spectra and those obtained for the as-received sample or the sample sputtered to a depth of 10 nm. The Sb 3d peak is normally the most intense peak observed in the XPS spectrum for antimony-containing materials, and this peak appears as a doublet (that is, Sb 3d_{5/2} and Sb 3d_{3/2}) because of spin-orbit splitting [7, 15]. The Sb 3d_{5/2} peak is the more intense peak in the

Sb 3d doublet and hence would be the preferred peak for quantification purposes and for chemical state identification. However, the Sb 3d_{5/2} peak is unfortunately completely overlapped by the intense O 1s peak in antimony/oxygen-containing materials like GSR (see Figure 7). Therefore, it is necessary to use the less intense Sb 3d_{3/2} peak for chemical state identification of antimony [15, 16]. Three oxides of Sb are known to exist: Sb₂O₃ (Sb³⁺), Sb₂O₄ (Sb⁴⁺), and Sb₂O₅ (Sb⁵⁺). For the direct-deposit GSR particulate examined in this study, the observed binding energies for the Sb 3d_{3/2} spectra were characteristic of Sb₂O₃ [15, 16] on the as-received sample and both of the argon ion sputtered samples. There was no evidence for the presence of Sb metal or other Sb oxides in any of the Sb 3d_{3/2} spectra.

Representative high-resolution Ba 3d and X-ray induced Ba MNN Auger spectra obtained for the GSR on ceramic sample after argon ion sputtering to a depth of 20 nm are shown in Figure 7. It has been reported that assessing the chemical state of Ba can be somewhat difficult because of the small chemical shifts typically observed in the Ba 3d peaks between the metallic and oxide states [12]. However, the X-ray induced Ba MNN Auger peak does show distinct differences between the metal and oxide. In this study, the observed binding energies and peak shapes for Ba 3d and MNN Auger peaks were characteristic of BaO (the only known form of Ba oxide), where barium is in the Ba²⁺ oxidation state [15, 16]. Similar Ba XPS spectra were obtained for the as-received sample and for the sample that

Table 2: XPS binding energies (eV) and chemical state assignments for a direct-deposit GSR sample on a ceramic substrate before and after argon ion sputtering.

XPS Peak	As-received		10-nm Argon Ion Sputter		20-nm Argon Ion Sputter	
	Binding Energy (eV)	Chemical State Assignment	Binding Energy (eV)	Chemical State Assignment	Binding Energy (eV)	Chemical State Assignment
Sb 3d _{3/2}	539.7	Sb ₂ O ₃	539.3	Sb ₂ O ₃	539.4	Sb ₂ O ₃
Ba 3d _{5/2}	780.2	BaO	780.1	BaO	780.2	BaO
Ba MNN	902.2		901.9		901.8	
Pb 4f _{7/2}	138.6	PbO	138.3 + lower B.E. shoulder	PbO + Pb metal	138.3 + lower B.E. shoulder	PbO + Pb metal

**Figure 6:** High-resolution Pb 4f XPS spectra for a direct-deposit GSR layer on a ceramic substrate: (A) as-received; (B) after a 10-nm argon ion sputter; and (C) after a 20-nm argon ion sputter.

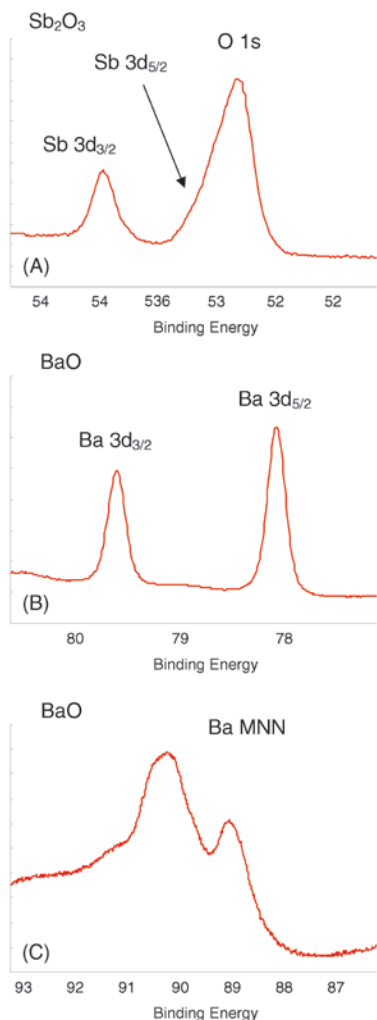


Figure 7: High-resolution XPS spectra for a direct-deposit GSR layer on a ceramic substrate after a 20-nm argon ion sputter: (A) Sb 3d and O 1s region, (B) Ba 3d region, and (C) X-ray-induced Ba MNN Auger region.

was argon ion sputtered to a depth of 10 nm. As was the case for Sb, there was no evidence for the presence of Ba metal in any of the Ba 3d spectra.

Summary

This study demonstrates that XPS is a valuable complementary technique for electron microscopy studies. XPS can provide important information regarding the surface composition and surface chemistry of multi-component particulate materials such as GSR. XPS results indicated that the three marker elements for GSR, that is, Pb, Sb, and Ba, are primarily present as PbO and Pb metal, Sb₂O₃, and BaO, respectively. The relative amounts of Sb and Ba in GSR increase relative to Pb with sputtered depth. Future planned studies will involve the collection and XPS analysis of GSR from a shooter's hands immediately after discharge of a firearm. Such data will illustrate the similarities and differences between

GSR particles collected in the present primer-only tests and particles produced from the actual discharge of a full cartridge from a firearm.


References

- [1] GM Wolten, RS Nesbitt, AR Calloway, GL Loper, and PF Jones, "Final Report on Particle Analysis for Gunshot Residue Detection," The Aerospace Corporation, El Segundo, CA, ATR-77 (7915)-3, 1977.
- [2] WL Tillman, *J Forensic Sci* 32 (1987) 62–71.
- [3] RS White and AD Owens, *J Forensic Sci* 32 (1987) 1595–1603.
- [4] D DeGaetano and JA Siegel, *J Forensic Sci* 35 (1990) 1087–95.
- [5] AJ Schwoeble and DL Exline, *Current Methods in Forensic Gunshot Residue Analysis*, CRC Press, Boca Raton, FL, 2000.
- [6] GE Frost, *Ammunition Making—An Insider's Story*, The National Rifle Association, Fairfax, VA, 1990.

- [7] JF Watts and J Wolsethholme, *An Introduction to Surface Analysis by XPS and AES*, John Wiley & Sons Ltd, Chichester, West Sussex, 2003.
- [8] DR Baer and MH Engelhard, *J Electron Spectrosc Related Phenom*, 178(79) (2010) 415–32.
- [9] DR Baer, DJ Gasper, P Nachimuthu, SD Techane, and DG Castner, *Anal Bioanal Chem* 396 (2010) 983–1002.
- [10] AJ Schwoeble, BR Strohmeier, and JD Piasecki, *Proc SPIE* 7729 (2010) 772916-1–772916-16.
- [11] JF Watts, *Surf Interface Anal* 42 (2010) 358–62.
- [12] M D'Uffizi, G Falso, GM Ingo, and G Padeletti, *Surf Interface Anal* 34 (2002) 502–06.
- [13] J Coumbaros, KP Kirkbride, G Klass, and W Skinner, *Forensic Sci Int* 119 (2001) 72–81.
- [14] P Collins, J Coumbaros, G Horsley, B Lynch, KP Kirkbride, W Skinner, and G Klass, *J Forensic Sci* 48 (2003) 538–53.
- [15] JF Moulder, WF Stickle, PE Sobol, and KD Bomben, *Handbook of X-ray Photoelectron Spectroscopy*, Perkin-Elmer Corporation, Eden Prairie, MN, 1992.
- [16] CD Wagner, AV Naumkin, A Kraut-Vass, JW Allison, CJ Powell, and JR Rumble, Jr., "NIST X-ray Photoelectron Spectroscopy Database," Version 3.5, National Institute for Standards and Technology, Gaithersburg, MD, 2003. Available online at: <http://srdata.nist.gov/xps/Default.aspx>.


MT

Minus K® Technology's Negative-Stiffness vibration isolators have been selected for ground testing of the James Webb Space Telescope (JWST).



Why have over 2,000 scientists in 35 countries selected Minus K® vibration isolators?

Our Negative Stiffness systems deliver 10x to 100x better performance than air systems and even better than active systems



Without Minus K® With Minus K®

The best performance and the lowest price. That's hard to beat!

minus k® TECHNOLOGY

460 S. Hindry Ave., Unit C, Inglewood, CA 90301
Tel: 310-348-9656 Fax: 310-348-9638
sales@minusk.com • www.minusk.com

Mention code MT0311 to get a 5% discount on our standard bench top or SM models